

Two-dimensional Numerical Estimation of Stress Intensity Factors and Crack Propagation in Linear Elastic Analysis

Abdulnaser M. Alshoaibi^{1,2}, M. S. A. Hadi², and A. K. Ariffin²

Abstract: An adaptive finite element method is employed to analyze two-dimensional linear elastic fracture problems. The mesh is generated by the advancing front method and the norm stress error is taken as a posteriori error estimator for the h -type adaptive refinement. The stress intensity factors are estimated by a displacement extrapolation technique. The near crack tip displacements used are obtained from specific nodes of natural six-noded quarter-point elements which are generated around the crack tip defined by the user. The crack growth and its direction are determined by the calculated stress intensity factors as the maximum circumference theory is also been involved in determining the direction. In evaluating the accuracy of the estimated stress intensity factors, five cases are tested consisting compact tension specimen, three-points bending specimen, double edge notched plate, central cracked plate and single edge cracked plate. These comprehensive tests are carried out and compared to the results from other studies. The crack trajectories for all of these specimen tests are also illustrated.

Keyword: linear elastic fracture mechanics, adaptive refinement, stress intensity factors, crack propagation

1 Introduction

The used of crack propagation laws based on stress intensity factor range is the most successful engineering application of fracture mechanics. This characterizes the stress intensity factors as of

the most important parameter in fracture analysis. In the elastic fracture analysis, the stress intensity factors sufficiently define the stress field close to the crack tip and provide fundamental information of how the crack is going to propagate. Basically, the estimation methods can be categorized into two groups, those based on field extrapolation near the crack tip and those which make use of the energy release when the crack propagates. The latter group includes the J -contour integration, the virtual crack extension and the strain energy release rate method. The main disadvantage of these methods is that the stress intensity factor components, K_I and K_{II} in mixed mode problems are either impossible or very difficult to be separated. Nevertheless, the first groups which are based on near-tip field fitting procedures require finer meshes to produce a good numerical representation of crack-tip fields. Usually, the singular point elements are generated to facilitate the calculation (Guinea, Planan and Elices 2000).

In general, numerical methods such as the Boundary Element Method (BEM) and the Finite Element Method (FEM) are used in the fracture analysis of structures, because of the complex shape and continuously changing path of the growing crack. A comprehensive review of the boundary element method for crack propagation can be referred to Aliabadi 1997. The finite element method has also been proven to be very well suited for the study of fracture mechanics, nevertheless modelling the propagation of a crack through a finite element mesh turns out to be difficult because of the modification of the mesh topology. Nodal relaxation is frequently used to release nodes, in order to enable the crack tip to propagate through the mesh. In adaptive mesh refinement, most analysts favour either the De-

¹ Corresponding author. Tel. +603-89216136. Fax. +603-89259659 E-mail address: alshoaibi@gmail.com; alhager01@yahoo.com (A. Alshoaibi).

² Department of Mechanical & Materials Engineering, Universiti Kebangsaan Malaysia, 43600 Bangi, Selangor Darul Ehsan, Malaysia.

launay technique or the advancing front method over other techniques when generating meshes due to the quality of unstructured meshes generated (El-Hamalawi 2004). Phongthanapanich and Dechaumphai (2004) used a finite element method with the adaptive Delaunay triangulation as mesh generator to analyze two-dimensional crack propagation problems. They described the Delaunay triangulation procedure consisting of mesh generation, node creation, mesh smoothing, and adaptive remeshing, all with object-oriented programming. They also used the displacement extrapolation method to determine the values of stress intensity factors for compact tension specimen, central cracked plate and single edge cracked plate for certain geometries only. In order to improve the accuracy of the near-tip stress fields, elements around the crack tip have their mid-side nodes displaced from their nominal positions to quarter points (Barsoum 1976, Barsoum 1977). The stress intensity factors are then calculated from the extrapolated nodal displacements on the crack faces next to the crack tip (Chan and Tuba 1970). Rao and Rahman (2000) developed the coupled meshless-finite element method for analyzing linear-elastic cracked structures subject to mode I and mixed mode condition. Their method was applied to calculate mode I and mode II stress intensity factors in a number of two-dimensional cracked structures.

The main objective of this paper is to determine the stress intensity factor for crack propagation problem under linear elastic fracture analysis using the displacement extrapolation technique with adaptive finite element method. The computational code is written in FORTRAN. The mesh for finite elements is the unstructured type; generated using the advancing front method. The global h -type adaptive mesh is adopted based on the norm stress error estimator. The quarter-point singular elements are uniformly generated around the crack tip in the form of rosette. The displacement extrapolation technique used in the calculation is explained. The algorithm is assessed by considering five standard test specimen geometries, i.e. compact tension specimen, three points bending specimen, double edge notched plate, central

cracked plate, and single edge cracked plate.

2 Mesh Generation and Adaptive Refinement

In this work, the unstructured triangle mesh is automatically generated by employing the advancing front method (Löhner 1997). This adopted technique however requires generating background mesh in order to accurately control the distribution of the geometrical characteristics such as the element size, element stretching and stretching directions for the new mesh. The background does not have to be precisely representing the geometry; however the accuracy of the distribution depends on this excellence and it must be completely cover the computational domain (Zienkiewicz, Taylor and Zhu 2005). The strategy taken to generate the background mesh is to utilize all the initial boundary nodes of geometry and construct the boundary triangles as the background mesh by the dichotomy technique. In this technique the computational domain must be a polygon since the boundary triangulations are carried out by means of dividing and repeating dividing the polygon into two subsets until the simplest polygon subsets i.e. the boundary triangles yielded. Therefore, if there are any internal boundaries representing for example holes, then connector lines must be introduced connecting each internal boundary to the external boundary. This will force the internal boundaries to be part of continuous line of the externals and therefore set the computational domain to be a polygon. In order to do this, the orientation direction of internal boundaries is set clockwise while for external boundary is set the other way round. The connector line is introduced by finding the nearest distance between any internal boundary points to any of the external ones (Sezer and Zeid 1991).

In the proposed dichotomy method, the division starts at any first found boundary point with large face angle and setting an angle range for searching the nearest nonadjacent point to be connected by a division line. The angle range is set in such the division is capable to produce high quality polygon subset shape. If the search for the nearest nonadjacent point failed then the division can be initiated at a boundary point with smaller face an-

gle. The classification for the face angle size θ_i based on the precedence is set as $\pi \leq \theta_1 < 2\pi$, $\pi/2 < \theta_2 < \pi$, $0 < \theta_3 \leq \pi/2$.

In order to properly represent the field singularity around the crack tip, the singular elements have to be constructed as well. Since the advancing front method generates the triangle elements starting from the boundary faces, the area around the crack tip for the construction of the singular elements is supposed to be isolated. This area is isolated by first generating nodes around the crack tip in the rosette form and then the crack tip node and the jointed boundary segments are removed. New boundary segments are then introduced linking all the new nodes to temporarily 'cut out' the template area from the original domain. Subsequently the advancing front triangulation can be executed. Finally singular elements are 'patched' into the rosette template to complete the process. This procedure as illustrated by Fig. 1 is almost similar to as has been proposed by Phongthanapanich and Dechaumphai (2004). The numbers of elements depend on the distributed nodes around the crack tip, which can be set by user. Here the natural triangular quarter point elements (Freese and Tracey 1976) are used instead of the collapse quadrilateral element proposed by Barsoum (1976).

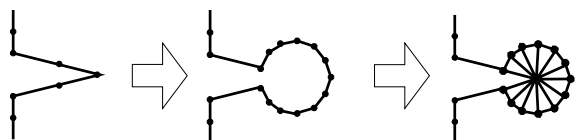


Figure 1: The cut and patch procedure of generating singular elements around a crack tip.

Fig. 2 shows example geometry where the whole process of generating the mesh is illustrated for better understanding. Fig. 2a illustrates the geometry of a plate with six holes and two notches. Fig. 2b shows six connector lines forcing the internal boundaries to be the continuous part of the external boundary. Fig. 2c shows the cutting out of the rosette templates around each crack tip. The background mesh for this domain is then set up automatically using dichotomy technique as shown in Figure 2d. Figure 2e shows the con-

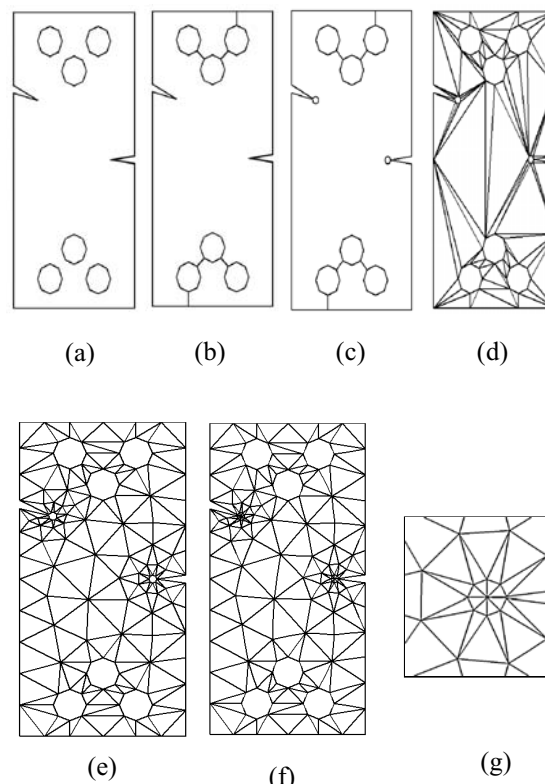


Figure 2: The mesh generation stages with inclusion of quarter point elements. The aspect ratio of the subfigures is not preserved.

ventional mesh being generated by the advancing front method. The first generation produces mesh with initial size set by user. Later, during adaptive refinement, this first generated mesh will be taken as the background mesh. In Fig. 2f, for each rosette template, quarter-point elements are then constructed. Fig. 2g shows the enlargement of the quarter-point element at one of the crack tip.

In general, the smaller mesh size gives more accurate finite element approximate solution. However, reduction in the mesh size leads to greater computational effort. The adaptive mesh refinement is employed as the optimization scheme. This scheme bases on a posteriori error estimator which is obtained from the solution from the previous mesh. Here stress error norm is taken as the error estimator. The strategy used to refine the mesh during analysis process is adopted from (Ariffin 1995) as follows:

- (i) Determine the error norm for each element

$$\|e\|^e = \int_{\Omega^e} (\sigma - \sigma^*)^T (\sigma - \sigma^*) d\Omega \quad (1)$$

where σ is the stress field obtained from the finite element calculation and σ^* is the smoothed stress field.

- (ii) Determine the average error norm over the whole domain

$$\|\hat{e}\| = \frac{1}{m} \sum_{e=1}^m \int_{\Omega^e} \sigma^T \sigma d\Omega \quad (2)$$

where m is the total number of elements in the whole domain.

- (iii) Determine a variable,
- ε_e
- for each element as

$$\varepsilon_e = \frac{1}{\eta} \frac{(\|e\|^e)^{1/2}}{(\|\hat{e}\|)^{1/2}} \quad (3)$$

where η is a percentage that measures the permissible error for each element. If $\varepsilon_e > 1$ the size of the element is reduced and vice versa.

- (iv) The new element size is determined as

$$\hat{h}_e = \frac{h_e}{(\varepsilon_e)^{1/p}} \quad (4)$$

where h_e is the old element size and p is the order of the interpolation shape function.

3 Stress Intensity Factor and Crack Propagation

In this paper, the displacement extrapolation method (Phongthanapanich and Dechaumphai (2004)) is used to calculate the stress intensity factors as follows:

$$K_I = \frac{E}{3(1+\nu)(1+\kappa)} \sqrt{\frac{2\pi}{L}} \left[4(v'_b - v'_d) - \frac{(v'_c - v'_e)}{2} \right] \quad (5)$$

$$K_{II} = \frac{E}{3(1+\nu)(1+\kappa)} \sqrt{\frac{2\pi}{L}} \left[4(u'_b - u'_d) - \frac{(u'_c - u'_e)}{2} \right] \quad (6)$$

where E is the modulus of elasticity, ν is the Poisson's ratio, κ is the elastic parameter defined by

$$\kappa = \begin{cases} (3-4\nu) & \text{plane stress} \\ (3-4\nu)/(1+\nu) & \text{plane strain} \end{cases}$$

and L is the quarter-point element length. The u' and v' are the displacement components in the x' and y' directions, respectively; the subscripts indicate their position as shown in Fig. 3.

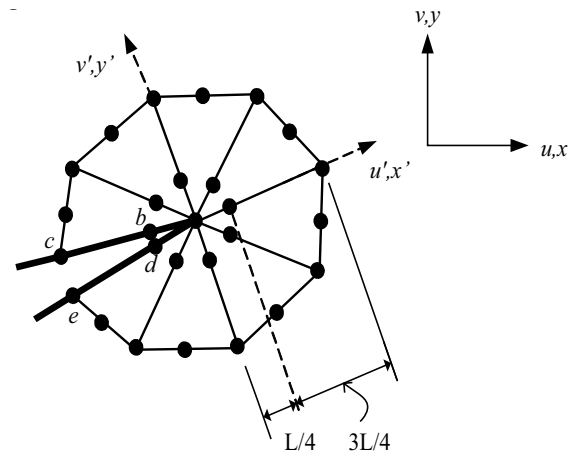


Figure 3: The quarter-point singular elements around the crack tip.

In order to simulate crack propagation under linear elastic condition, the crack path direction must be determined. There are several methods use to predict the direction of crack trajectory such as the maximum circumferential stress theory, the maximum energy release rate theory and the minimum strain energy density theory.

The maximum circumferential stress theory asserts that, for isotropic materials under mixed-mode loading, the crack will propagate in a direction normal to maximum tangential tensile stress. In polar coordinates, the tangential stress is given by

$$\sigma_\theta = \frac{1}{\sqrt{2\pi r}} \cos \frac{\theta}{2} \left[K_I \cos^2 \frac{\theta}{2} - \frac{3}{2} K_{II} \sin \theta \right] \quad (7)$$

The direction normal to the maximum tangential stress can be obtained by solving $d\sigma_\theta/d\theta = 0$ for θ . The nontrivial solution is given by

$$K_I \sin \theta + K_{II} (3 \cos \theta - 1) = 0 \quad (8)$$

which can be solved as:

$$\theta_0 = \pm \cos^{-1} \left\{ \frac{3K_{II}^2 + K_I \sqrt{K_I^2 + 8K_{II}^2}}{K_I^2 + 9K_{II}^2} \right\} \quad (9)$$

In order to ensure that the opening stress associated with the crack direction of the crack extension is maximum, the sign of θ_0 should be opposite to the sign of K_{II} (Andersen 1998). The two possibilities are illustrated in Fig. 4.

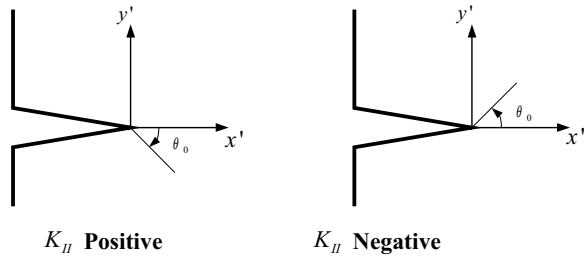


Figure 4: Sign of the propagation angle

The criterion for crack to propagate from crack tip is based on the material toughness, K_C . If the calculated stress intensity factor, $K_I \geq K_C$ then the crack will propagate to the direction θ_0 expressed by Equation (9). The crack increment length Δa is taken 10%-20% of the initial crack length a , inversely proportional to the ratio of K_{II}/K_I . The ratio represents the mixed mode proportionality, therefore shorter increment length should be taken to carefully justify the crack path curvature when K_{II} is relatively large compare to K_I (Bittencourt, Wawrzynek, Ingraffea, Sousa (1996)).

4 Numerical Analysis and Validation

In order to carry out a comprehensive evaluation of the stress intensity factors approximated by the developed program, five well-known plate geometries, compact tension specimen, three-points bending specimen, double edge notched plate, central cracked plate, and single edge cracked

plate are being considered. The crack propagation trajectory for these geometries is also predicted to evaluate the performance of the developed program.

4.1 Compact Tension Specimen

The compact tension test specimen geometry and the final adaptive mesh are shown in Fig. 5. The specimen has an initial crack length $a = 9\text{cm}$, width $W = 18.8\text{cm}$, and the thickness B , has various values as explain bellows.

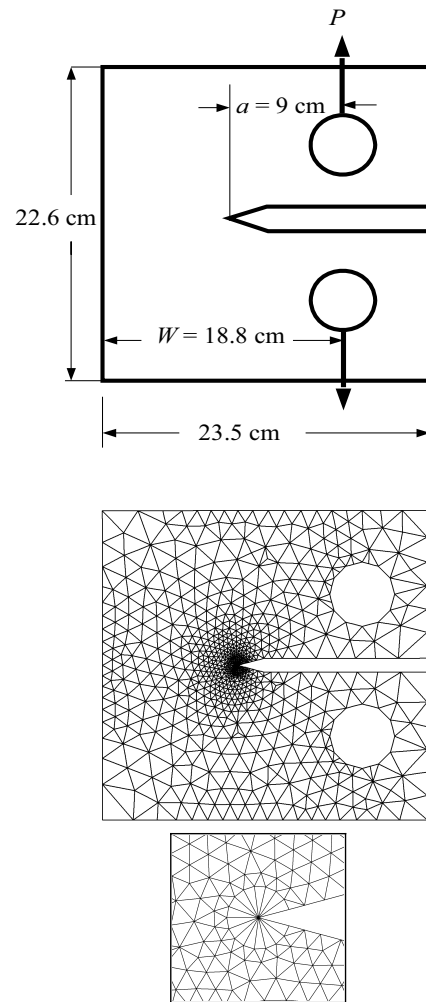


Figure 5: Compact tension geometry, the final adaptive mesh and the enlargement of mesh around crack tip.

The analytical stress intensity factor for this geometry can be calculated from Anderson (1994)

as follows:

$$K_I = P \left(2 + \frac{a}{W} \right) \left(0.886 + 4.64 \left(\frac{a}{W} \right) - 13.32 \left(\frac{a}{W} \right)^2 + 14.72 \left(\frac{a}{W} \right)^3 - 5.6 \left(\frac{a}{W} \right)^4 \right) / B\sqrt{W} \left(1 - \frac{a}{W} \right)^{3/2} \quad (10)$$

where P is the applied load.

The computed values of the stress intensity factor under plane stress condition are compared with the experimental and numerical results which obtained from Parnas and Bilir (1996) as shown in Figs. 6-9. In the study, steel and aluminum plates with their respective modulus of elasticity 210GPa and 70GPa, and Poisson's ratio 0.3 and 1/3, are used. There are three different thicknesses 6.0, 8.3, and 13.6mm for the steel specimens, however only one thickness of 5mm is considered for the aluminum specimen. The experimental results are compared with finite element results using ANSYS software as shown in Fig. 6. The comparison also comprises the analytical solution as shown in Figs. 6-9. The results of the steel specimens show the effect of the variation for the three thicknesses on the stress intensity factors.

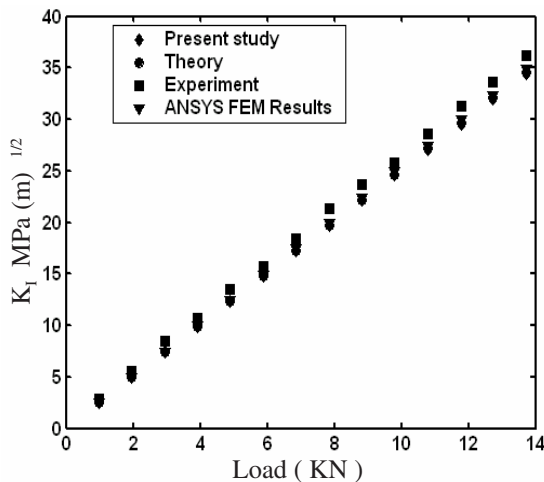


Figure 6: Stress intensity factor values for steel specimen, $B=8.3\text{mm}$.

The present values of stress intensity factors are very close to the theoretical solutions and are in

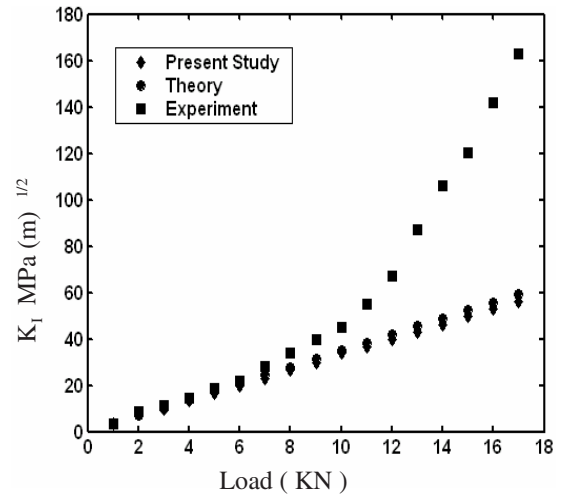


Figure 7: Stress intensity factor values for steel specimen, $B=6.0\text{mm}$.

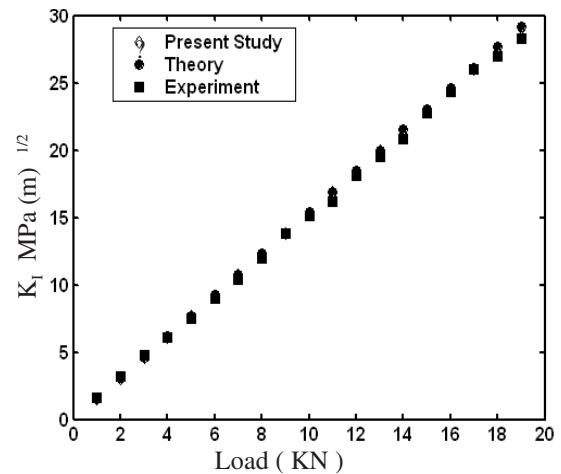


Figure 8: Stress intensity factor values for steel specimen, $B=13.6\text{mm}$.

good agreements with the experimental results except in Fig. 7, there is a deviation beyond 10 KN load. This deviation might be due to the plastic deformations around the crack tip.

Fig. 10 shows four steps of crack propagation for the compact tension specimen. The predicted crack propagation seems to follow the mode I trajectory very well.

4.2 Three Points Bend Specimen

The geometry of the three points bend specimen and the final adaptive mesh with are shown in Fig

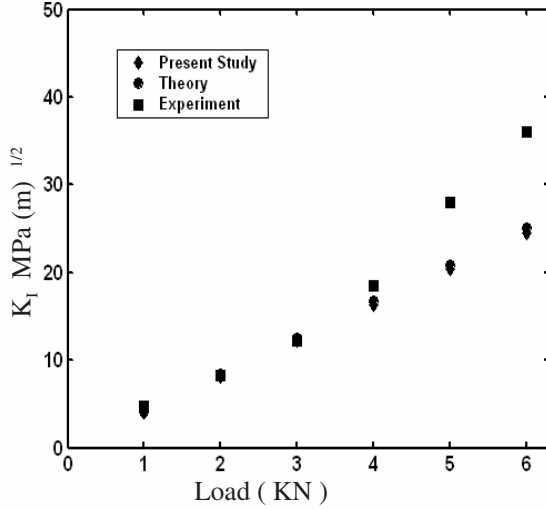


Figure 9: Stress intensity factor values for aluminum specimen, $B=5.0\text{mm}$.

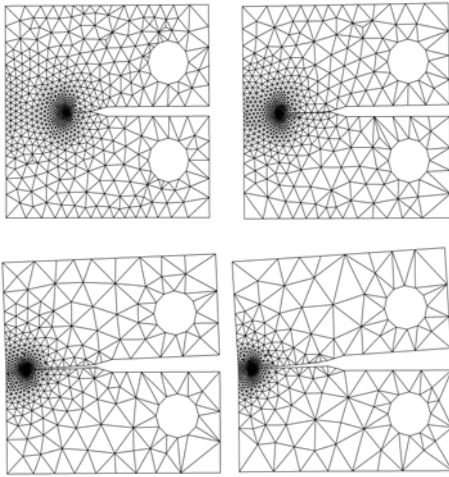


Figure 10: The crack propagation trajectory for a compact tension specimen under mode I loading.

11. The analytical stress intensity factor for this problem can be calculated from Broek (1986) as:

$$K_I = \frac{PS}{BW^{\frac{3}{2}}} \left[2.9 \left(\frac{a}{W} \right)^{\frac{1}{2}} - 4.6 \left(\frac{a}{W} \right)^{\frac{3}{2}} + 21.8 \left(\frac{a}{W} \right)^{\frac{5}{2}} - 37.6 \left(\frac{a}{W} \right)^{\frac{7}{2}} + 38.7 \left(\frac{a}{W} \right)^{\frac{9}{2}} \right] \quad (11)$$

The geometry is imposed by plane strain condition with point load P , span length S , height W , thickness B and crack length a .

The dimensionless stress intensity factor for this specimen is given by Freese and Barrata (2006) as:

$$\bar{K}_I = \left(1 - \frac{a}{W} \right)^{3/2} K_I BW / 6P \quad (12)$$

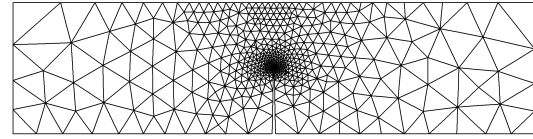
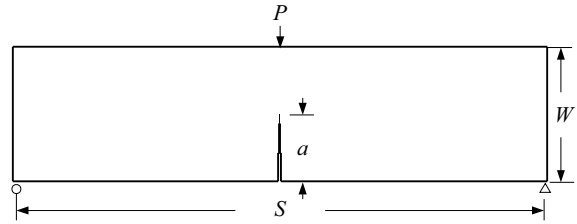


Figure 11: Three points bend specimen and the final adaptive mesh.

The results from present study, the experimental results obtained from Wei and Zhao (1997) and values from ASTM (1991) standard formula are compared together as shown in Tab. 1. The comparison exhibits an adequate agreement between all methodologies adopted.

Furthermore, the comparison of results from this paper and those obtained from references (Freese and Baratta (2006), Orange (1988), and Fett(1998)) are shown in Table 2 for $S/W = 4$. The dimensionless form of the estimated stress intensity factor is obtained by Eq. (12). Freese and Baratta provide values for a range of $0 < a/W < 1.0$. Meanwhile, Orange (1988) investigated the three point bend stress intensity factors for short cracks (i.e. $a/W \leq 0.5$) and specifically examined the effect of contact stress due to the center-point load on such factors. Fett (1998) presents for a range of $0.1 < a/W < 0.8$. The results in the present study seem very well close to those of references.

Fig. 12 shows four steps of crack propagation for the three points bend specimen. Clearly, the pre-

Table 1: Comparison of stress intensity factors for three points bend specimen

| Loads (KN) | K_I (MPa(m) ^{1/2}) | | | | |
|------------|--|-------------------|------------------------------------|-------------|---------------|
| | Experimental results Wei and Zhao (1997) | | | ASTM (1991) | Present study |
| | Two strain gage | Three strain gage | Two strain gage different position | | |
| 1.96 | 9.7108 | 7.604145 | 8.76422 | 8.37 | 8.179 |
| 3.92 | 18.59874 | 14.339283 | 17.193421 | 16.73 | 16.452 |
| 5.88 | 29.16369 | 25.54176 | 25.99356 | 25.1 | 24.539 |
| 7.84 | 38.87382 | 35.143038 | 34.440378 | 33.46 | 32.719 |
| 9.80 | 48.99547 | 44.661891 | 43.331697 | 41.83 | 40.899 |

Table 2: Comparisons of dimensionless stress intensity factors for three points bend specimen.

| (a/W) | Freese and Baratta (2006) | Orange (1988) | Fett (1998) | Present study |
|-------|---------------------------|---------------|-------------|---------------|
| 0.1 | 0.832 | 0.837 | 0.850 | 0.821 |
| 0.2 | 0.700 | 0.697 | 0.704 | 0.6978 |
| 0.3 | 0.612 | 0.609 | 0.609 | 0.601 |
| 0.35 | 0.576 | 0.575 | – | 0.565 |
| 0.4 | 0.545 | 0.545 | 0.545 | 0.535 |
| 0.45 | 0.518 | 0.519 | – | 0.5101 |
| 0.5 | 0.494 | 0.494 | 0.498 | 0.48936 |
| 0.55 | 0.475 | – | – | 0.471 |
| 0.6 | 0.459 | – | 0.463 | 0.4526 |
| 0.7 | 0.433 | – | 0.433 | 0.430 |
| 0.8 | 0.410 | – | 0.408 | 0.40 |
| 0.9 | 0.384 | – | – | 0.3827 |

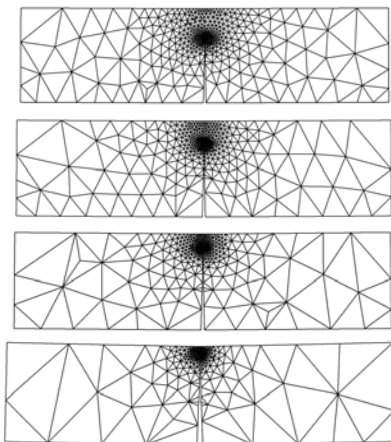


Figure 12: The crack propagation trajectory for a three points bend specimen under mode I loading.

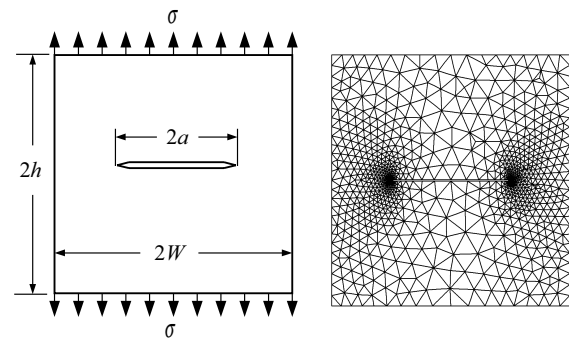


Figure 13: Central crack plate and the final adaptive mesh

dicted crack opening very well justifies the pure mode I trajectory pattern.

4.3 Central Cracked Plate

The geometry of the central cracked plate and the final adaptive mesh are shown in Fig. 13. The notations for the geometry dimension and crack length are same as for the previous specimen and σ is a far field stress. The ratio of the height h to the width W is 1.

The analytical stress intensity factor for this problem can be calculated from Tada, Paris and Irwin (2000).

$$K_I = \sigma \sqrt{\pi a} \left[\sec \left(\frac{\pi a}{2W} \right) \right]^{1/2} \cdot \left[1 - 0.025 \left(\frac{a}{W} \right)^2 + 0.06 \left(\frac{a}{W} \right)^4 \right] \quad (13)$$

The dimensionless stress intensity factor is given by Maiti, Mukhopadhyay and Kakodkar (1997) as

Table 3: Dimensionless stress intensity factor for central crack

| (a/W) | $K_I/(\sigma\sqrt{\pi a})$ | | | |
|-------|---|--|--------------------|---------------|
| | Matos et al. (2004) DBEM, singularity subtraction | Portela et al. (1992) DBEM, J-integral | Tada et al. (2000) | Present study |
| 0.4 | 1.118 | 1.114 | 1.109 | 1.0900 |
| 0.6 | 1.312 | 1.308 | 1.303 | 1.2747 |
| 0.8 | 1.816 | 1.815 | 1.816 | 1.8131 |

follows:

$$\bar{K}_I = K_I/(\sigma\sqrt{\pi a}) \quad (14)$$

Table 3 shows the comparison between the results of stress intensity factors of present study to those from Matos, Moreira, Portela and Castro (2004) which are estimated using dual boundary element method (DBEM) with the implementation of post processing singularity subtraction technique, the results of DBEM using J -integral method obtained by Portela, Aliabadi and Rooke (1992) and the analytical solutions of Tada, Paris and Irwin (2000). As shown in this table, the agreement is obviously good.

For other ratio of a/W , Tab. 4 shows the comparison between the results obtained in the present study and those calculated by Eq. (13).

Table 4: Dimensionless stress intensity factor for central cracked plate

| (a/W) | $K_I/(\sigma\sqrt{\pi a})$ | |
|-------|----------------------------|---------------|
| | Tada et al.(2000) | present study |
| 0.1 | 1.0059 | 1.001 |
| 0.2 | 1.0244 | 1.02368 |
| 0.3 | 1.05613 | 1.04156 |
| 0.5 | 1.1862 | 1.1879 |
| 0.7 | 1.4873 | 1.4655 |
| 0.9 | 2.5766 | 2.565 |

Tab. 5 shows the comparison of the present results and the numerical results using boundary element method with modified crack closure integral which were presented by Maiti, Mukhopadhyay and Kakodkar (1997) as a comparison to the analytical solution given by Murakami (1987).

In this table one can see that the present results are closer the analytical solution than those from Maiti, Mukhopadhyay and Kakodkar (1997).

Table 5: Dimensionless stress intensity factor for central crack plate

| (a/W) | $K_I/(\sigma\sqrt{\pi a})$ | | |
|-------|----------------------------|--------------|---------------|
| | Murakami (1987) | Maiti (1997) | Present study |
| 0.2 | 1.0254 | 1.0116 | 1.02368 |
| 0.3 | 1.0594 | 1.0408 | 1.04156 |
| 0.4 | 1.1118 | 1.0906 | 1.0900 |
| 0.5 | 1.1891 | 1.1644 | 1.1879 |
| 0.6 | 1.3043 | 1.2721 | 1.2747 |
| 0.7 | 1.4842 | 1.4440 | 1.4655 |
| 0.8 | 1.7989 | 1.7449 | 1.8131 |

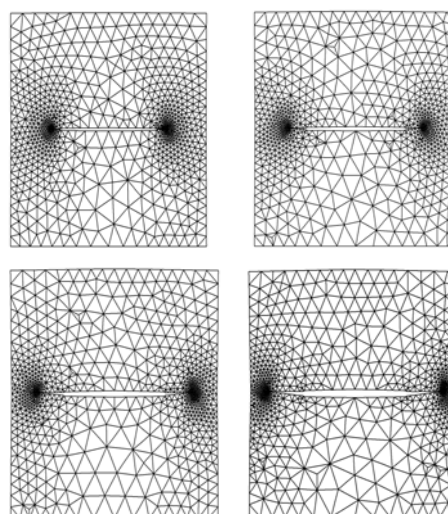


Figure 14: The crack propagation trajectory for a central crack specimen under mode I loading

Fig. 14 shows four steps of central crack propagation for the initial crack length ratio $a/W=0.5$, the predicted crack propagation resembles the experimental results Simonsen and Tornqvist (2004).

4.4 Double Edge Notched Plate

The geometry of the double edge notched plate specimen and the final adaptive mesh are shown in Fig. 15. Here, the ratio of specimen height h to the width W is $5/3$.

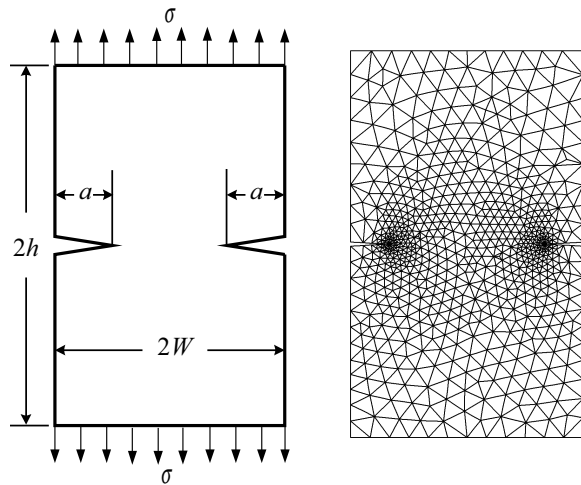


Figure 15: Double edge notched plate and the final adaptive mesh

The analytical stress intensity factor for this problem can be calculated from Tada, Paris and Irwin (2000) as:

$$K_I = \frac{\sigma\sqrt{\pi a}}{\sqrt{1-\frac{a}{W}}} \left[1.122 - 0.561 \left(\frac{a}{W}\right) - 0.205 \left(\frac{a}{W}\right)^2 + 0.471 \left(\frac{a}{W}\right)^3 - 0.190 \left(\frac{a}{W}\right)^4 \right] \quad (15)$$

The non-dimensional stress intensity factor is given by Zhu and Smith (1995) as follows:

$$\bar{K}_I = K_I / (\sigma\sqrt{\pi a}) \quad (16)$$

The present results for various initial crack lengths shown in Table 6 exhibit close agreement to the analytical solutions calculated by Eq. (15).

Fig. 16 shows four steps of central crack propagation for $a/W=0.5$. The crack propagates towards

the expected path under mode I loading condition.

Table 6: Dimensionless stress intensity factor for double edge notched plate

| (a/W) | $K_I / (\sigma\sqrt{\pi a})$ | |
|-------|------------------------------|---------------|
| | Tada et al. (2000) | present study |
| 0.1 | 1.1198 | 1.1166 |
| 0.2 | 1.1215 | 1.1218 |
| 0.3 | 1.1288 | 1.1260 |
| 0.4 | 1.1465 | 1.8930 |
| 0.5 | 1.1812 | 1.1829 |
| 0.6 | 1.2439 | 1.2483 |
| 0.7 | 1.3561 | 1.3560 |
| 0.8 | 1.5727 | 1.5731 |
| 0.9 | 2.1116 | 2.1113 |

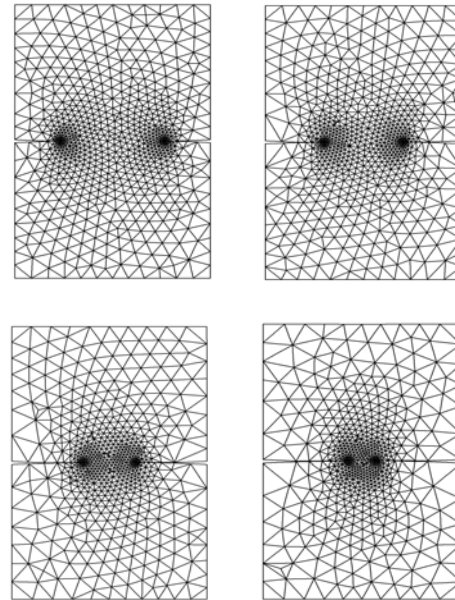


Figure 16: The crack propagation trajectory for a double edge notched plate under mode I loading.

4.5 Single Edge Cracked Plate

The single edge cracked geometry and the final mesh is shown in Fig. 17. This plate is subjected to far-field shear stress $\tau = 1\text{N/cm}^2$ along the top edge while is being fixed at the bottom edge. The initial crack length is $a=3.5\text{cm}$, the height

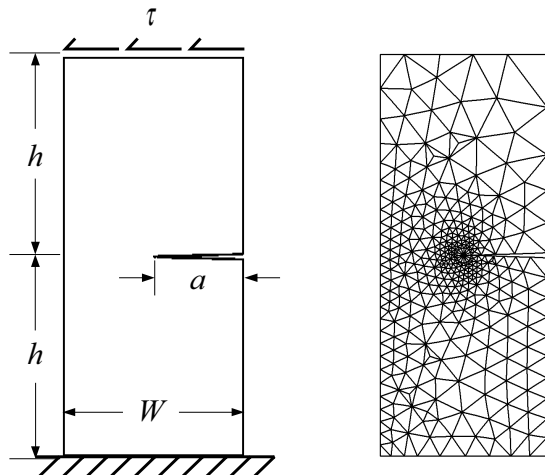


Figure 17: The single edge cracked plate and the final adaptive mesh

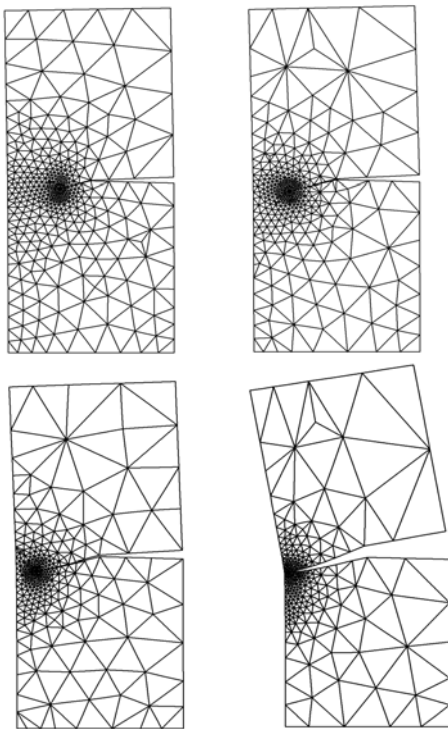


Figure 18: The single edge cracked plate deformation and crack propagation

$2h = 16\text{cm}$, the width $W = 7\text{ cm}$ and the thickness $B = 1\text{cm}$

The plane strain condition is assumed in the analysis. The computed stress intensity factors K_I and K_{II} are $33.55\text{N/cm}^{3/2}$ and $4.50\text{N/cm}^{3/2}$ comparing to $34.00\text{ N/cm}^{3/2}$ and $4.55\text{N/cm}^{3/2}$ from Phongthanapanich and Dechaumphai (2004) respectively.

Fig. 18 shows the predicted deformation and crack growth direction. The prediction of crack direction is shown only for a mixed mode case. This however, sufficient to show the capability of the program, since both mode I and II cases are inherent in this case. The crack propagation closely resembles the simulation trajectory of Rao and Rahman (2000).

5 Conclusions

The adaptive finite element method using advancing front method for crack propagation analysis and stress intensity factors prediction was presented. The norm stress error is taken as a posterior estimator for the h -type adaptive refinement. The nodes of natural six-node quarter point elements which are generated around the crack tip, were employed to form a circular zone surrounding the tip in order to better capture the stress field. The adaptive remeshing technique places small elements around the crack tips and in region with large change of stress gradients. Larger elements are generated in other regions to minimize the total number of unknowns and the computational time.

The accuracy of the estimated stress intensity factors has been evaluated through the assessments comprising five standard specimens. The results of stress intensity factors are compared to the closed form solutions and to the extensive results of other studies. The crack simulations for mode I and mixed mode cases show the acceptable crack path predictions. The results of the assessments strongly indicate that the finite element simulation for two-dimensional linear elastic fracture mechanics problems has been successfully employed.

References

- Aliabadi, M.H.** (1997): A new generation of boundary element methods in fracture mechanics. *International Journal of Fracture*, vol.86, pp.91-125.
- Andersen, M.R.** (1998): Fatigue crack initiation and growth in ship structures. Ph.D Dissertation, *Technical University of Denmark*.

- Anderson, T.L.** (1994): *Fracture mechanics: fundamental and applications*. 2nd Edition: CRC Press.
- Ariffin, A.K.** (1995): Powder compaction, finite element modelling and experimental validation, PhD Thesis, *University of Wales Swansea*.
- ASTM- standard E399-90** (1991): standard test methods for plane strain fracture toughness of metallic materials, ASTM.
- Barsoum, R.S.;** (1976): On the use of isoparametric finite element in linear fracture mechanics, *International Journal of Numerical Methods in Engineering*, vol. 10, pp. 25-37.
- Barsoum, R.S.;** (1977): Triangular quarter-point elements as elastic and perfectly-plastic crack tip element, *International Journal of Numerical Methods in Engineering*, vol. 11, 1, pp. 85-98.
- Bittencourt, T.N.; Wawrzynek, P.A.; Ingraffea, A.R.; Sousa, J.L.;** (1996): Quasi-automatic simulation of crack propagation for 2D LFM problems. *Engineering Fracture Mechanics*, vol. 55, no. 2, pp. 321-334
- Broek, David** (1986): *Elementary engineering fracture mechanics*. 4th Edition; Martinus Nijhoff Publishers.
- Chan, S.K.; Tuba, I.S.; Wilson, W.K.;** (1970): On the finite element method in linear fracture mechanics, *Engineering Fracture Mechanics*, vol. 2, pp.1-17.
- El-Hamalawi, A.;** (2004): A 2d combined advancing front-delaunay mesh generation scheme, *Finite Element in Analysis and Design*, vol. 40, pp.967-989.
- Fett T.** (1998): Stress intensity factors for edge-cracked plates under arbitrary loading. *Fatigue Fracture Engineering Materials and Structures*. Vol. 22, pp. 301-305.
- Freese Colin E.; Barrata Francis I.** (2006): Single edge-crack stress intensity factor solutions. *Engineering Fracture Mechanics*, vol. 73, pp. 616-625.
- Freese, C.E.; Tracey, D.M.;** (1976): The natural triangle versus collapsed quadrilateral for elastic crack analysis. *International Journal of Fracture*, vol. 12, pp. 767-770.
- Guinea, G.V.; Planan, J.; Elices, M.** (2000): K_I evaluation by the displacement extrapolation technique. *Engineering Fracture Mechanics*, vol. 66, pp.243-255.
- Löhner R.** (1997): Automatic unstructured grid generators, finite element in analysis and design, vol. 25, pp. 111-134.
- Maiti, S.K; Mukhopadhyay, N.K.; Kakodkar, A.** (1997): Boundary element method based computation of stress intensity factor by modified crack closure integral. *Computational Mechanics*, vol. 19, pp. 203-210.
- Matos, P. F .P.; Moreira, P.M.; Portela, A.; Castro, P.M.** (2004): Dual boundary element analysis of cracked plates: post-processing implementation of the singularity subtraction technique. *Computers and Structures*, vol. 82, pp. 1443-1449.
- Murakami, Y.** (1987): *Stress intensity factors handbook*. Pergamon Press.
- Orange, T.W.** (1988): Stress intensity and crack displacement for small edge cracks. *NASA Technical Paper 2801*.
- Parnas, L.; Bilir, O.G.** (1996): Strain gage methods for measurement of opening mode stress intensity factor. *Engineering Fracture Mechanics*, vol. 55, 3, pp. 485-492.
- Phongthanapanich, S. ;Dechaumphai, P.** (2004): Adaptive delaunay triangulation with object-oriented programming for crack propagation analysis. *Finite Element in Analysis and Design*, vol. 40, pp.1753-1771.
- Portela, A.; Aliabadi, M.H.; Rooke** (1992): Dual boundary element method: effective implementation for crack problems. *International Journal of Numerical Methods in Engineering*, vol. 33, pp. 1269-1287.
- Rao, B.N. ; Rahman, S.** (2000): An efficient meshless method for fracture analysis of cracks. *Computational Mechanics*, vol. 26, no. 4, pp. 398-408
- Sezer, L.; Zeid I.** (1991): Automatic quadrilateral/triangular free form mesh generation for planar region. *International Journal for Numerical Methods in Engineering*, vol. 32, pp. 1441-1483.

Simonsen, B.C., Tornqvist, R., 2004. Experimental and numerical modelling of ductile crack propagation in large-scale shell structures. *Marine Structures*, vol. 17, no. 1, pp. 1-27.

Tada, H.; Paris, P.C.; Irwin, G.R. (2000): *The Stress Analysis of Cracks Handbook*, ASME Press, New York.

Wei, J.; Zhao, J.H. (1997): A two-strain gage technique for determining mode I stress intensity factor. *Theoretical and Applied Fracture Mechanics*, vol. 28, pp. 135-140.

Zhu, W.X.; Smith, D.J. (1995): On the use of displacement extrapolation to obtain crack tip singular stresses and stress intensity factors, *Engineering Fracture Mechanics*, vol. 51, no. 3, pp. 391-400.

Zienkiewicz, O.C.; Taylor, R.L.; Zhu, J.Z. (2005): *The finite element method: its basis and fundamentals*. 6th Edition 2005: Elsevier Butterworth-Heinemann.

